Reliable Potential Energy Surfaces for the Reactions of H_2O with ThO_2, PaO_2^+, UO_2^{2+}, and UO_2^+

Monica Vasiliu,[a] Kirk A. Peterson,[b] John K. Gibson,[c] and David A. Dixon[a]

[a] Department of Chemistry, The University of Alabama, Shelby Hall, Tuscaloosa, Alabama 35487-0336, USA

[b] Department of Chemistry, Washington State University, Pullman WA 99164-4630 USA

[c] Chemical Sciences Division, Lawrence Berkeley National Laboratory, Berkeley, California 94720, USA

Abstract

The potential energy surfaces for the reactions of H_2O with ThO_2, PaO_2^+, UO_2^{2+}, and UO_2^+ have been calculated at the coupled cluster CCSD(T) level extrapolated to the complete basis set limit with additional corrections including scalar relativistic and spin orbit. The reactions proceed by the formation of an initial Lewis acid-base adduct $(H_2O)AnO_2^{0/+/2+}$ followed by a proton transfer to generate the dihydroxide $AnO(OH)_2^{0/+/2+}$. The results are in excellent agreement with mass spectrometry experiments and prior calculations of hydrolysis reactions of the Group 4 transition metal dioxides MO_2. The differences in the energies of the stationary points on the potential energy surface are explained in terms of the charges on the system and the populations on the metal center. The use of an improved starting point for the coupled cluster CCSD(T) calculations based on density functional theory with the PW91 exchange-correlation functional or Brueckner orbitals is described. The importance of including second order spin orbit corrections for closed

shell molecules is also described. These improvements in the calculations are correlated with the *5f* populations on the actinide.

Keywords: actinyl reactions, coupled cluster CCSD(T), relativistic quantum chemistry, hydrolysis

Introduction

Hydrolysis reactions of metal oxides play an important role in the initial steps of the conversion of metal oxides to compounds containing OH groups. For example, there is substantial interest in how the oxygen atoms in actinyl ions exchange with water in solution. The first experiments of this phenomenon were reported in 1949 and have continued to recent times with additional experimental and computational studies.[1,2,3,4,5,6,7,8,9,10,11,12,13,14,15] An important concept is the role of AnO_2^+ with the An in the +5 oxidation state. Rios et al. provided detailed insights into the exchange mechanism as well as to periodic variations for these types of reactions.[16] They showed that exchange in the gas phase proceeds in the order of UO_2^+ > NpO_2^+ > PuO_2^+ on the basis of $^{16}O/^{18}O$ labelled mass spectrometry experiments and density functional theory calculations at the B3LYP/6-311++G(d,p)/Stuttgart-ECP and PBE/TZP-ZORA levels. They showed that the reaction potential energy surface proceeded by the initial formation of a Lewis acid-base adduct of the H_2O with the AnO_2^+ ion followed by proton transfer to form the species $An(O)(OH)_2^+$. In the experiments, exchange is monitored by reacting $H_2{}^{18}O$ with $An^{16}O_2$ and monitoring the location of the ^{18}O by mass spectrometry; in the computations any $^{16}O/^{18}O$ isotope mass effect was assumed to be negligible, as also in the present work. The barrier for the initial proton transfer step is lowest for U and highest for Pu. The $An(O)(OH)_2^+$ dihydroxyl complex was found to be higher in energy than the Lewis acid-base adduct in all cases with $UO(OH)_2^+$ being the most stable exchange intermediate relative to the $UO_2^+ + H_2O$ reactant asymptote. The predicted initial transition state for proton transfer showed that the barrier was 3 kcal/mol above the reactant asymptote at the B3LYP level, but this was considered to be within the error of the DFT calculations. A second smaller barrier was found for the rearrangement of the $An(^{16}O)(^{16}OH)(^{18}OH)^+$ intermediate so that the ^{18}OH and actinyl ^{16}O could exchange

isotopes. Effectively, this second barrier exchanges an axial OH for an equatorial OH. For U, this barrier was less than 1 kcal/mol. The potential energy surface for UO_2^{2+} was also studied and, as expected, the initial Lewis acid-base interaction energy was much larger than for the monocation and the proton transfer barrier was much larger, 57 kcal/mol vs 37 kcal/mol for the monocation. However, the much larger complexation (physisorption) energy of 66 kcal/mol for the dication vs. 33 kcal/mol for the monocation means that the initial proton transfer barrier for the dication is below the reactant asymptote. In addition, the $An(O)(OH)_2^{+(2+)}$ intermediate is 22 kcal/mol above the initial Lewis acid-base adduct for the dication and 12 kcal/mol above for the monocation. The second small barrier to exchange O isotopes is ~ 4 kcal/mol for the dication as compared to < 1 kcal/mol for the monocation. Dau et al. recently extended this work to study the reaction of PaO_2^+ with H_2O and found experimentally that the Lewis acid-base adduct and dihydroxyl complex were essentially isoenergetic.[17]

We have been exploring the reactions of H_2O with related transition metal oxide molecules and nanoclusters and have found similar types of potential energy surfaces.[18,19,20] In the current work, we have expanded our study to the early actinides and have studied the addition of H_2O to ThO_2, PaO_2^+, and UO_2^{2+} to understand how the trends observed previously for the +5 actinyls depend on the oxidation state changing from +IV to +VI. We also studied the hydrolysis reaction of UO_2^+ as well. We have performed these calculations at a much higher level than previously reported, the coupled cluster CCSD(T)/CBS (complete basis set) level for the energetics based on CCSD(T) or MP2 geometries. These studies have been enabled by the development of the new correlation-consistent basis sets with effective core potentials for Th and U[21] and a new suite of comparable basis sets for Pa is presented here. The recent experimental results enable a benchmark of the computed energetics for the reaction of PaO_2^+ with H_2O. The

current results are the first potential energy surfaces to be reported for the actinides at the CCSD(T)/CBS level.

Computational Details

We used coupled-cluster methods at the CCSD(T)[22,23,24,25] (coupled cluster theory with single and double excitations with a perturbative triples correction) level with aug-cc-pV*n*Z (H and O)[26,27] and cc-pV*n*Z-PP (Th, Pa, and U)[21,28,29,30] basis sets with *n* = D, T, and Q (abbreviated as aV*n*Z) and CCSD(T) including core-valence (CV) correlation corrections with the aug-cc-pwCV*n*Z[31] and cc-pwCV*n*Z-PP basis set for *n* = D, T, and Q (abbreviated as awCV*n*Z) to predict the structural characteristics and thermodynamic properties of the reactions of ThO_2, PaO_2^+, $^2UO_2^+$, and UO_2^{2+} with water. Equilibrium geometries of stable structures were optimized at the CCSD(T)/aV*n*Z level with *n* = D and T and reoptimized at the CCSD(T)(CV)/awCV*n*Z level with *n* = D and T. Transition states were optimized at the frozen core MP2 (second order Møller-Plesset) level[32,33] with the aug-cc-pV*n*Z basis set for *n* = D and T using Gaussian09.[34] Single point CCSD(T)/aV*n*Z and CCSD(T)(CV)/awCV*n*Z for *n* = D, T, and Q calculations were performed at the MP2 optimized geometries for the transition states. The open-shell calculations were done with the R/UCCSD(T) approach where a restricted open shell Hartree-Fock (ROHF) calculation was initially performed and the spin constraint was then relaxed in the coupled cluster calculation.[24,35,36,37] The CCSD(T) total energies were extrapolated to the CBS limit by fitting to a mixed Gaussian/exponential (Eq. 1):[38]

$$E(n) = E_{CBS} + A \exp[-(n-1)] + B \exp[-(n-1)^2] \quad (1)$$

where *n* = 2, 3, and 4 (aVDZ through aVQZ and awCVDZ through awCVQZ).

Using the optimized geometries described above, all-electron CCSD(T) calculations using the 3rd-order Douglas-Kroll-Hess Hamiltonian[39,40,41] were also carried out using the aug-

cc-pV*n*Z-DK (H and O)[42] and cc-pV*n*Z-DK3 (Th and U)[21] basis sets with n = D, T, and Q. Calculations with correlation of the actinide 5s, 5p, and 5d electrons were carried out using the aug-cc-pwCVnZ-DK (O) and cc-pwCVnZ-DK (Th and U) basis sets. The DK3 CBS limits were obtained using Eq. (1) with n = D through Q basis sets. Effects on the relative energetics due to spin-orbit coupling were calculated using completely uncontracted aug-cc-pVDZ/cc-pVDZ-DK3 basis sets and the exact two-component (X2C) Hamiltonian,[43,44] which contains atomic-mean-field 2-electron spin-same-orbit corrections. Calculations for the closed shell molecules containing Th, Pa^+, and U^{2+} were carried out at the relativistic CCSD(T) level of theory,[45] while those for the open shell molecules containing U^+ utilized the Fock-space CCSD method.[46,47] The latter employed orbitals from the closed-shell UO_2^{2+} cases, which defined the (0,0) sectors. The active space in these latter calculations to which electrons were attached corresponded to the U 7s and 5f orbitals, and in all cases a virtual orbital cutoff of 12.0 a.u. was employed. All SO calculations were carried out with the DIRAC13 program[48] with the default Gaussian nuclear model.

The CCSD(T) calculations, except as discussed above for the spin orbit corrections, were performed with the MOLPRO 2012 program package.[49,50] The calculations were performed on our local (UA and WSU) Opteron-based and Xeon-based Linux clusters, and the Opteron-based Linux cluster in the Molecular Science Computing Facility in the William R. Wiley Environmental Molecular Sciences Laboratory at the Pacific Northwest National Laboratory.

Results and Discussion

Geometries The H_2O adds to the metal dioxide $MO_2^{0/+/2+}$ to form a Lewis acid-base complex $(H_2O)MO_2^{0/+/2+}$. A proton transfer can then occur to generate $MO(OH)_2^{0/+/2+}$. The geometries (Figure 1 and Table 1) show some interesting variations. The geometries of $Th(O)(OH)_2$ and $Pa(O)(OH)_2^+$ are pyramidal with C_s symmetry with the two OH groups equivalent. Thus, there is

Table 1. Optimized Geometry Parameters for $MO_2^{0/+/2+}$, $(H_2O)MO_2^{0/+/2+}$, and $MO(OH)_2^{0/+/2+}$.[a]

Molecule	Point Group	r(M-O)	r(M-O(H_2)/M-O(H))	r(O-H)	∠O-M-O/ (H)O-M-O(H)	∠O-M-O(H2)/ O-M-O(H)
ThO_2	C_{2v}	1.905(x2)			117.0	
$ThO_2(H_2O)$	C_1	1.959, 1.934	2.601	0.985, 0.968	114.1	71.6, 93.6
$ThO(OH)_2$	C_s	1.901	2.165(x2)	0.956(x2)	107.8	111.4
PaO_2^+	$D_{\infty h}$	1.776			180.0	
$PaO_2(H_2O)^+$	C_{2v}	1.788(x2)	2.447	0.966(x2)	180.0	90.0(x2)
$PaO(OH)_2^+$	C_s	1.798	2.023	0.964(x2)	98.5	113.8(x2)
UO_2^{2+}	$D_{\infty h}$	1.700			180.0	
$UO_2(H_2O)^{2+}$	C_{2v}	1.712(x2)	2.321	0.976(x2)	180.0	90.0(x2)
$UO(OH)_2^{2+}$	C_s	1.721	1.941 eq, 1.899 ax	0.981 eq, 0.988 ax	91.6	99.9 eq, 168.5 ax
$^2UO_2^+$	$D_{\infty h}$	1.760			180.0	
$^2UO_2(H_2O)^+$	C_{2v}	1.789(x2)	2.453	0.970(x2)	180.0	90.0(x2)
$^2UO(OH)_2^+$	C_s	1.792	2.026eq, 2.017ax	0.966 eq, 0.971 ax	90.5	108.3 eq, 161.2 ax

[a] Bond distances in Å and bond angles in degrees. Geometries optimized at the CCSD(T)//awT/wT-PP level except for $ThO_2(H_2O)$, $^2UO_2(H_2O)^+$, and $^2UO(OH)_2^+$ optimized at CCSD(T)//awD/wD-PP

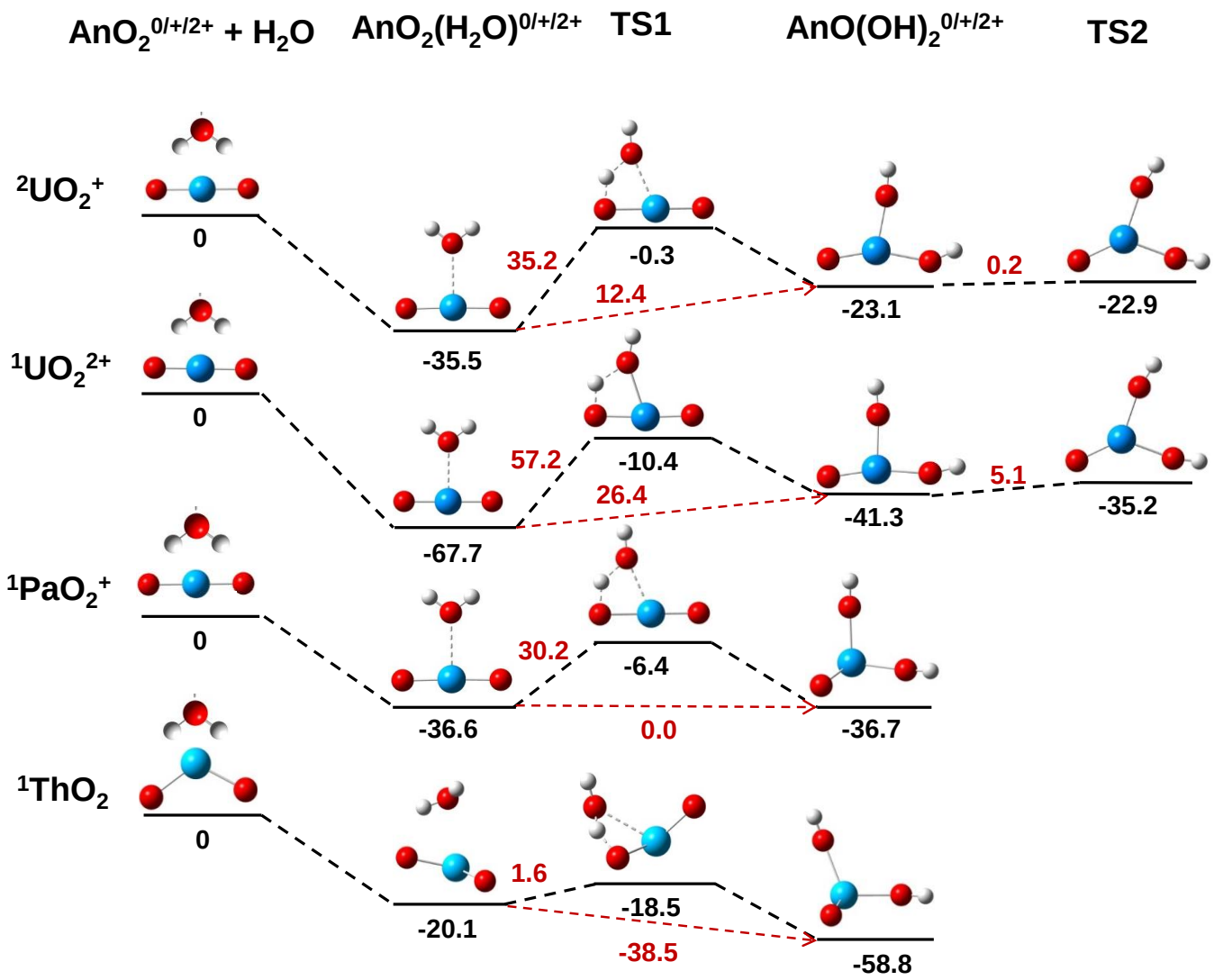

Figure 1. ΔH_{298} (kcal/mol) relative to the reactant asymptotes. Values in red are relative energies for individual steps. The oxygen is red, the hydrogen is white and the An is blue.

Table 2. Calculated Values for ΔH_{298} for $ThO_2 + H_2O \rightarrow ThO_2(H_2O) \rightarrow ThO(OH)_2$ (TS) $\rightarrow ThO(OH)_2$ in kcal/mol.

Method	Geometry	$(H_2O)ThO_2$	$ThO(OH)_2(TS)$[a]	$ThO(OH)_2$	ΔH	$\Delta H^{\ddagger}$
valence only						
CCSD(T)/CBS(avnz)	Up to CCSD(T)/aT/T	-20.5	-18.8	-58.9	-38.4	1.7
FC-CBS(avnz)/DK	CCSD(T)/aT/T	-20.1	-18.4	-58.0	-37.8	1.8
FC-CBS(avnz)/DK + SO	CCSD(T)/aT/T	-20.2	-18.3	-57.9	-37.7	1.9
CCSD(T)/CBS(avnz)/PW91	CCSD(T)/aT/T	-20.6	-19.0	-59.1	-38.5	1.6
CCSD(T)/CBS(avnz)/PW91+SO	CCSD(T)/aT/T	-20.7	-18.9	-59.0	-38.3	1.8
BCCD(T)/CBS(avnz)/PW91	CCSD(T)/aT/T	-20.5	-18.8	-59.0	-38.5	1.7
BCCD(T)/CBS(avnz)/PW91 +SO[b]	CCSD(T)/aT/T	-20.6	-18.7	-58.9	-38.3	1.8
include core-valence						
FC-CBS(avnz)+CV/DK	CCSD(T)/aT/T	-20.4	-18.6	-58.7	-38.3	1.7
FC-CBS(avnz)+CV/DK + SO	CCSD(T)/aT/T	-20.4	-18.5	-58.6	-38.2	1.9
CCSD(T)/CBS(awcvnz)	Up to CCSD(T)/awT/wT[c]	-20.4	-19.2	-59.6	-39.2	1.2
CV-CBS(awcvnz)/DK	CCSD(T)/awT/wT	-19.9	-18.4	-58.5	-38.7	1.5
CV-CBS(awcvnz)/DK + SO	CCSD(T)/awT/wT	-19.9	-18.3	-58.5	-38.5	1.6
CCSD(T)/CBS(awcvnz)/PW91	CCSD(T)/awT/wT[c]	-20.5	-19.4	-59.7	-39.2	1.1
CCSD(T)/CBS(awcvnz)/PW91+SO	CCSD(T)/aT/T	-20.6	-19.3	-59.6	-39.1	1.3
BCCD(T)/CBS(awcvnz)/PW91	CCSD(T)/awT/wT[c]	-20.4	-19.2	-59.7	-39.3	1.2
BCCD(T)/CBS(awcvnz)/PW91+SO	CCSD(T)/awT/wT	-20.4	-19.1	-59.6	-39.1	1.3
ECP correction[d]		0.5	0.8	1.1		
CCSD(T)/CBS(awcvnz)/PW91+SO +ECP correction		-20.1	-18.5	-58.6	-38.5	1.6

[a]TS opt at MP2/aT/T-PP [b]same value with HF starting psi [c] $ThO_2(H_2O)$ opt at CCSD(T)/awD/wD. [d] ECP corrections = CV-CBS(wcvnz)/DK- CCSD(T)/CBS(awcvnz)

Table 3. Calculated Values for ΔH_{298} for $PaO_2^+ + H_2O \rightarrow PaO_2^+(H_2O) \rightarrow PaO(OH)_2^+$ (TS) $\rightarrow PaO(OH)_2^+$ in kcal/mol.

Method	Geometry	$(H_2O)PaO_2^+$	$PaO(OH)_2^+$ (TS)[a]	$PaO(OH)_2^+$	ΔH	$\Delta H^{\dagger}$
valence only						
CCSD(T)/CBS(avnz)	Up to CCSD(T)/aT/T	-36.3	-6.3	-36.0	0.2	30.0
FC-CBS(avnz)/DK	CCSD(T)/aT/T	-35.7	-5.3	-35.1	0.7	30.4
FC-CBS(avnz)/DK + SO	CCSD(T)/aT/T	-36.1	-6.2	-36.5	-0.4	29.9
CCSD(T)/CBS(avnz)/PW91	CCSD(T)/aT/T	-36.5	-6.8	-37.3	-0.8	29.7
CCSD(T)/CBS(avnz)/PW91+SO	CCSD(T)/aT/T	-36.8	-7.6	-38.7	-1.9	29.2
BCCD(T)/CBS(avnz)/PW91	CCSD(T)/aT/T	-36.3	-6.2	-36.0	0.3	30.1
BCCD(T)/CBS(avnz)/PW91 +SO[b]	CCSD(T)/aT/T	-36.7	-7.1	-37.4	-0.7	29.6
include core-valence						
FC-CBS(avnz)+CV/DK	CCSD(T)/aT/T	-36.2	-5.3	-34.1	2.1	30.9
FC-CBS(avnz)+CV/DK + SO	CCSD(T)/aT/T	-36.6	-6.2	-35.5	1.1	30.4
CCSD(T)/CBS(awcvnz)	Up to CCSD(T)/awT/wT	-36.8	-6.5	-36.0	0.8	30.3
CV-CBS(awcvnz)/DK	CCSD(T)/awT/wT	-36.1	-5.1	-33.9	2.2	31.0
CV-CBS(awcvnz)/DK + SO	CCSD(T)/awT/wT	-36.5	-5.9	-35.3	1.2	30.6
CCSD(T)/CBS(awcvnz)/PW91	CCSD(T)/awT/wT	-37.0	-7.1	-37.4	-0.4	29.9
CCSD(T)/CBS(awcvnz)/PW91+SO	CCSD(T)/awT/wT	-37.3	-7.9	-38.8	-1.4	29.4
BCCD(T)/CBS(awcvnz)/PW91	CCSD(T)/awT/wT	-36.8	-6.5	-36.0	0.8	30.3
BCCD(T)/CBS(awcvnz)/PW91+SO	CCSD(T)/awT/wT	-37.2	-7.3	-37.4	-0.3	29.8
ECP correction [c]		0.7	1.5	2.1		
CCSD(T)/CBS(awcvnz)/PW91+SO +ECP correction		-36.6	-6.4	-36.7	0.0	30.2

[a] TS opt at MP2/aT/Stutt. [b] same value with HF starting psi. [c] ECP corrections = CV-CBS(wcvnz)/DK- CCSD(T)/CBS(awcvnz)

Table 4. Calculated Values for ΔH_{298} for ΔH_{298} for $UO_2^{2+} + H_2O \rightarrow UO_2^{2+}(H_2O) \rightarrow UO(OH)_2^{2+}$ (TS) $\rightarrow UO(OH)_2^{2+}$ in kcal/mol.

Method	Geometry	$(H_2O)UO_2^{2+}$	$UO(OH)_2^{2+}$ (TS1)[a]	$UO(OH)_2^{2+}$	$UO(OH)_2^{2+}$ (TS2)[a]	ΔH	$\Delta H^{\dagger}$ (1)	$\Delta H^{\dagger}$ (2)
valence only								
CCSD(T)/CBS(avnz)	Up to CCSD(T)/aT/T	-65.7	-6.4	-35.4	-34.5	30.3	59.3	0.9
FC-CBS(avnz)/DK	CCSD(T)/aT/T	-65.6	-5.8	-34.7	-29.5	30.9	59.8	5.1
FC-CBS(avnz)/DK + SO	CCSD(T)/aT/T	-66.3	-7.4	-37.1	-31.8	29.3	59.0	5.3
CCSD(T)/CBS(avnz)/PW91	CCSD(T)/aT/T	-66.5	-9.2	-39.0	-35.1	27.5	57.3	3.9
CCSD(T)/CBS(avnz)/PW91+SO	CCSD(T)/aT/T	-67.3	-10.9	-41.5	-37.4	25.8	56.4	4.1
BCCD(T)/CBS(avnz)/PW91	CCSD(T)/aT/T	-65.9	-7.0	-36.5	-32.3	29.3	58.9	4.2
BCCD(T)/CBS(avnz)/PW91+SO	CCSD(T)/aT/T	-66.6	-8.6	-39.0	-34.6	27.6	58.0	4.4
include core-valence								
FC-CBS(avnz)+CV/DK	CCSD(T)/aT/T	-66.2	-6.0	-35.0	-29.2	31.1	60.2	5.9
FC-CBS(avnz)+CV/DK + SO	CCSD(T)/aT/T	-66.9	-7.6	-37.5	-31.4	29.4	59.3	6.0
CCSD(T)/CBS(awcvnz)	Up to CCSD(T)/awT/wT	-66.4	-6.9	-36.1	-30.8	30.3	59.5	5.4
CV-CBS(awcvnz)/DK	CCSD(T)/awT/wT	-66.1	-5.7	-34.9	-28.8	31.3	60.4	6.0
CV-CBS(awcvnz)/DK + SO	CCSD(T)/awT/wT	-66.9	-7.3	-37.3	-31.1	29.6	59.6	6.2
CCSD(T)/CBS(awcvnz)/PW91	CCSD(T)/awT/wT	-67.2	-10.0	-40.1	-35.8	27.1	57.2	4.3
CCSD(T)/CBS(awcvnz)/PW91+ SO	CCSD(T)/awT/wT	-68.0	-11.6	-42.5	-38.1	25.4	56.4	4.4
BCCD(T)/CBS(awcvnz)/PW91	CCSD(T)/awT/wT	-66.6	-7.7	-37.5	-32.9	29.1	58.9	4.5
BCCD(T)/CBS(awcvnz)/PW91+ SO	CCSD(T)/awT/wT	-67.3	-9.3	-39.9	-35.2	27.4	58.0	4.7
ECP correction [c]		0.3	1.2	1.3	2.0			
CCSD(T)/CBS(awcvnz)/PW91+ SO +ECP correction		-67.7	-10.4	-41.3	-36.2	26.4	57.2	5.1

[a] TS opt at MP2/aT/Stutt. [b] same value with HF starting psi. [c] ECP corrections = CV-CBS(wcvnz)/DK- CCSD(T)/CBS(awcvnz)

Table 5. Calculated Values for ΔH_{298} for $^2UO_2^+ + H_2O \rightarrow {}^2UO_2^+(H_2O) \rightarrow {}^2UO(OH)_2^+$ (TS) $\rightarrow {}^2UO(OH)_2^+$ in kcal/mol.

Method	Geometry	$(H_2O)UO_2^+$	$UO(OH)_2^+$ (TS1)[a]	$UO(OH)_2^+$	$UO(OH)_2^+$ (TS2)[a]	ΔH	$\Delta H^\dagger$ (1)	$\Delta H^\dagger$ (2)
valence only								
CCSD(T)/CBS(avnz)	Up to CCSD(T)/aT/T	-34.6	0.6	-20.2	-19.9	14.4	35.1	0.3
FC-CBS(avnz)/DK	CCSD(T)/aT/T	-34.4	0.9	-19.7	-19.2	14.7	35.3	0.5
FC-CBS(avnz)/DK + SO	CCSD(T)/aT/T	-35.0	0.4	-20.8	-20.3	14.2	35.4	0.5
include core-valence								
FC-CBS(avnz)+CV/DK	CCSD(T)/aT/T	-34.7	0.8	-19.4	-18.8	15.4	35.6	0.5
FC-CBS(avnz)+CV/DK + SO	CCSD(T)/aT/T	-35.3	0.4	-20.4	-19.9	14.8	35.7	0.6
CCSD(T)/CBS(awcvnz)	Up to CCSD(T)/awT/wT[b]	-34.6	0.3	-20.0	-20.2	14.6	34.9	-0.1
CV-CBS(awcvnz)/DK	CCSD(T)/awT/wT	34.3	1.0	-18.9	-18.6	15.5	35.3	0.2
CV-CBS(awcvnz)/DK + SO	CCSD(T)/awT/wT	-34.8	0.6	-19.9	-19.7	14.9	35.4	0.2
CCSD(T)/CBS(awcvnz)/PW91	CCSD(T)/awT/wT[b]	-35.3	-0.6	-23.2	-23.4	12.1	34.7	-0.2
CCSD(T)/CBS(awcvnz)/PW91 +SO	CCSD(T)/awT/wT[b]	-35.8	-1.0	-24.3	-24.4	11.5	34.8	-0.1
ECP correction [c]		0.3	0.7	1.2	1.5			
CCSD(T)/CBS(awcvnz)/PW91 +SO +ECP correction		-35.5	-0.3	-23.1	-22.9	12.4	35.2	0.2

[a] TS opt at MP2/aD/D-PP [b] $^2UO_2(H_2O)^+$ and $^2UO(OH)_2^+$ opt at CCSD(T)/awD/wD. [c] ECP corrections = CV-CBS(wcvnz)/DK-CCSD(T)/CBS(awcvnz)

no transition state for the intermediate to exchange OH group positions so that $^{16}O/^{18}O$ isotope exchange can occur without any barrier once the proton is transferred from H_2O. In contrast, $U(O)(OH)_2^{2+}$ and $U(O)(OH)_2^{+}$ are planar with two inequivalent OH groups with one OH approximately axial and one approximately equatorial with respect to the remaining actinyl O.

The imaginary frequencies for the transition states are given in the Supporting Information. As would be expected, the imaginary frequencies for the initial proton transfer step are large with values between 1150 and 1350 cm^{-1} for ThO_2, 1520 to 1600 cm^{-1} for PaO_2^{+}, 1480 to 1730 cm^{-1} for UO_2^{2+}, and 1620 to 1725 cm^{-1} for UO_2^{+}. The ranges are due to the different computational levels used. For the closed shell systems, the MP2 imaginary frequencies are larger in magnitude than the B3LYP values and the reverse is true for open shell UO_2^{+}. The imaginary frequencies for the transition states for O isotope exchange are very small, <110 cm^{-1}, as the OH groups are moving in contrast to movement of a proton.

Relative Energy Calculations The important energies on the potential energy surface at a variety of computational levels for each reaction are given in Tables 2 to 5 for ThO_2, PaO_2^{+}, UO_2^{2+}, and UO_2^{+} and are summarized in Figure 1. A substantial number of energy calculations were performed at different computational levels to develop the best potential energy surfaces. The first set of calculations was performed with only the valence electrons correlated. These calculations were performed as follows. First, a typical calculation with the effective core potential and associated basis sets was performed. Then a CCSD(T) calculation was performed at the all-electron DK3 level followed by a spin orbit correction. We then followed this by changing the orbitals for the CCSD(T) from the normal Hartree-Fock ones to the use of those from density functional theory with the PW91 generalized gradient exchange-correlation functional.[51,52,53] These values were then corrected by the above spin orbit term. Another set of

calculations were done with Brueckner orbitals.[54,55,56,57,58,59] The DFT-initial point and Brueckner orbital calculations were performed to determine if an improved starting point for the CCSD(T) calculations improves the relative energies. It should be noted that in all cases the use of either PW91 or Brueckner orbitals resulted in much smaller values of the T_1 diagnostic. We then repeated the calculations with the core-valence basis sets to include the effects of core-valence corrections. The additional correlated electrons were the 1s on O and the 5s,5p,5d electrons on the actinide. The difference in the DK3 and ECP terms was used to calculate a correction for the effective core potential as

ECP correction = CV-CBS(awcvnz)/DK- CCSD(T)/CBS(awcvnz)

This correction together with the spin orbit correction was added to the CCSD(T)/CBS(awcvnz) core-valence energy starting from the PW91 orbitals to generate our best estimate of the potential energy surface shown in Figure 1.

The results for Th show that the relative energies for the initial Lewis acid-base adduct, transition state and dihydroxyl complex vary by about 1 kcal/mol between all of the different methods. The ECP correction is 0.5 kcal/mol for the Lewis acid-base adduct, 0.8 for the transition state and 1.0 for the dihydroxyl complex. There is effectively no spin orbit contribution for any of the three structures relative to ThO_2. There is also little change on the use of different orbitals for the CCSD(T) calculations.

The results for Pa(V) show that there is a comparable range of relative energies of about 1 kcal/mol for the initial Lewis acid-base adduct, just as for the Th Lewis acid-base adduct but that there is a much larger spread of values for the transition state and the dihydroxyl complex of up to 5 kcal/mol. The effective core potential corrections are larger for Pa and increase again from the Lewis acid-base adduct to the transition state to the dihydroxyl complex with the latter

having a correction of 2.1 kcal/mol. The spin orbit corrections are larger as well, with only a small correction for the Lewis acid-base adduct and a larger correction of 1.4 kcal/mol for the dihydroxyl complex. It is important to remember that these are all closed shell molecules and that the spin orbit correction is relative to the correction in the free ion PaO_2^+. Again, for the Lewis acid-base adduct, there are only small differences among the different orbital choices for the CCSD(T) calculations. The effect of using an improved set of orbitals for the CCSD(T) increases from the Lewis acid-base adduct to the transition state to the dihydroxyl complex, where the change for the latter is 1.4 kcal/mol when using the PW91 functional. In this case there is essentially no change from the HF orbital results when using Brueckner orbitals.

Changing the oxidation state of the central atom to U(VI) leads to comparable ECP corrections for the different structures as for Pa(V). The spin orbit corrections are now larger for all structures, being 0.7 kcal/mol for the initial Lewis acid-base adduct and 2.7 kcal/mol for the dihydroxyl complex. The use of PW91-based orbitals or the use of Brueckner orbitals leads to non-zero corrections even for the Lewis acid-base adduct. The use of PW91 orbitals leads to an additional Lewis acid-base adduct stabilization of 0.8 kcal/mol. A larger change of 3.0 kcal/mol is predicted for the first transition state, a stabilization of 4 kcal/mol is predicted for the dihydroxyl complex, and a correction of almost 5 kcal/mol is predicted for the second transition state.

For U(V), which is an open shell doublet, the ECP corrections are smaller than for Pa(V) and U(VI). The spin orbit corrections are also smaller with a maximum of 1.1 kcal/mol for the dihydroxyl complex. This suggests that the spin-orbit effects already present in $^1PaO_2^+$ are not changing very much when H_2O is added either as the Lewis acid-base adduct or as the dihydroxyl complex. The largest change from among the different orbital choices input to the

CCSD(T) calculations is 3 kcal/mol for the dihydroxyl complex and the transition state connecting the two dihydroxyl complexes. Overall, the changes are smaller in U(V) than in U(VI).

Potential energy surfaces The reaction profiles at the highest level of theory are given in Figure 1. The changes with actinide oxidation and charge state are interesting. The Lewis acid-base complexation energy for H_2O binding to Th in ThO_2 is -20 kcal/mol and can be considered as a physisorption energy. The formation of the intermediate from H_2O and ThO_2 can be considered to be a chemisorption energy and it is exothermic by -59 kcal/mol. The proton transfer barrier is very low, ~ 2 kcal/mol, so under ambient conditions the chemisorbed species will be formed readily with little of the physisorbed Lewis acid-base adduct being formed. These values can be compared to the results for H_2O binding to a ThO_2 surface.[60] For an initial coverage of 0.6 H_2O/nm^2, the experimental physisorption energy is -25 kcal/mol and our value is comparable to this, even though only a single ThO_2 molecule is present. The absolute value of the adsorption enthalpy decreases as coverage increases. Our value for chemisorption is consistent with the DFT PBE/plane wave prediction of -50 kcal/mol for the (100) surface of ThO_2.[60]

The change in oxidation state to +V for PaO_2^+ with the introduction of a positive charge leads to a significant change in the potential energy surface. The magnitude of the initial complexation energy increases to -37 kcal/mol, consistent with the presence of a positive charge. The chemisorbed intermediate is essentially isoenergetic with the adduct and the barrier for proton transfer from the adduct to the intermediate has increased to 30 kcal/mol. Again, there is no barrier in the intermediate for isotope exchange due to its inherent symmetry. The result that the adduct and the dihydroxyl complex are essentially isoenergetic is in good agreement with the experimental observations.[17]

The introduction of a second positive charge for the U in the +VI oxidation state leads to another significant increase in the magnitude of the complexation energy to -68 kcal/mol. The energy of the chemisorbed intermediate relative to the reactant asymptote for UO_2^{2+} is comparable to that for PaO_2^+. The barrier for proton transfer is much higher, 57 kcal/mol for the dication, consistent with the formation of a positive proton closer to the U(VI) center and increased repulsion.

The comparison of Pa(V) and U(V) shows that the initial complexation energies are comparable, with that for UO_2^+ being slightly smaller by 1 kcal/mol than that for PaO_2^+. This is consistent with the formal presence of a 5f electron on U(V) which can repel the lone pair from the O in the H_2O. However, the +1 charge interaction dominates so it is a small effect. The barrier to transfer the proton is 35 kcal/mol for U(V), about 5 kcal/mol higher than for PaO_2^+, again consistent with the formal presence of the single 5f electron in U(V). The proton transfer-barrier of $(H_2O)UO_2^+$ is just below the reactant asymptote, consistent with the observed oxo-exchange reactions.[16] The chemisorbed intermediate is now significantly higher in energy (12 kcal/mol) than the initial physisorption complex.

The H_2O + ThO_2 0 K binding energy to generate the Lewis acid-base adduct is smaller than those for binding H_2O to TiO_2, ZrO_2, and HfO_2 at 0 K, by 9 to 16 kcal/mol (at the CCSD(T)-DK/awCVTZ-DK level for Ti and at the CCSD(T)/CBS//B3LYP/aD level for Zr and Hf) as shown in Table 6.[19,20] The transition state for proton transfer for ThO_2 is comparable to the values for Zr and Hf and lower than that for Ti. The chemisorption energies to form the dihydroxyl complex for Ti, Zr, and Hf are all more exothermic than that for ThO_2. The energetics for the Group 4 transition metals follow the trend that the largest binding energy is associated with the metal with the most ionic metal character, i.e., Hf. Thus, the energies to form

Table 6. **M-O BDEs, Lewis acid-base complexation Energies relative to MO_2 + H_2O ($\Delta H(1)$), Chemisorption Energy to Form $MO(OH)_2^{0/+/2+}$ ($\Delta H(2)$), and the Barrier Height for the First Proton Transfer ($\Delta H^{\dagger}$) in kcal/mol at 0K**.

MO_2	Single BDE [a]	Ave BDE	$(H_2O)MO_2^{0/+/2+}$ $\Delta H(1)$	$MO(OH)_2^{0/+/2+}$ $\Delta H(2)$	TS $\Delta H^{\ddagger}$
ThO_2	163.5 ± 3.3[62]	186[62]	-19.4	-58.3	2.3
PaO_2^+	186.4 ± 6.9[62]	189[62]	-36.5	-36.5	31.0
UO_2^{2+}	126.4 ± 7.4[62]	148[62]	-67.3	-41.3	57.9
UO_2^+	177 ± 3.3[62]	181[62]	-35.3	-23.7	35.5
TiO_2	145.6[64]	149[63]	-30.3[20]	-70.6[20]	6.0[20]
ZrO_2	142[64]	164[63]	-27.5[19]	-75.8[19]	2.5[19]
HfO_2		157[63]	-34.6[19]	-86.9[19]	2.1[19]

[a] $MO_2^{0/+/2+} \rightarrow MO^{0/+/2+} + O$

the ThO_2 adduct and the dihydroxyl complex are the lowest in this series if ThO_2 is grouped with the Group 4 transition metals. We have previously shown that the average Th-F and Th-Cl bond dissociation energies (BDEs) for ThF_4 and $ThCl_4$ are the largest for the nominal Group 4 metals with the Ti-X BDEs being the lowest followed by the Zr-X BDEs and then the Hf-X BDEs.[61] These M-X bond energy trends are likely to be associated with the ease of ionization of the metal. In contrast, the chemistry of ThO_2 with H_2O does not follow the M-X bond energy trend.

An interesting question to address is whether there are any correlations between the M-O bond dissociation energies (BDEs) given in Table 6.[62,63,64] The average Th-O BDE as well as first M-O BDE for ThO_2 is higher than any of the Group 4 transition elements consistent with the least amount of energy being released for formation of the physisorbed adduct of ThO_2 with H_2O. The difference between the Th and Hf energies to form the dihydroxyl complex is about 29 kcal/mol, essentially the same as the difference in the average M-O BDEs. However, this cannot be the entire reason in the Group 4 metals, as the lowest BDE is for Ti and it also has less energy

released on forming the dihydroxyl complex than Zr or Hf. Thus the ability of the metal atom to stabilize OH binding also plays a role and here we expect the more ionic Hf(IV) to be better than Zr or Ti.

The actinyl ions clearly do not follow the same pattern as ThO_2 and the Group 4 MO_2 in terms of the energetics to form the dihydroxyl complex as the complex is comparable in energy to that of the adduct for PaO_2^+, about 12 kcal/mol higher in energy for UO_2^+, and 26 kcal/mol higher in energy for UO_2^{2+}.

Trends Across the Actinide Series: Experiment and Theory As was recently reported,[17] the properties of the gas-phase adduct of PaO_2^+ and H_2O indicate that the physisorbed hydrate and chemisorbed hydroxide are sufficiently close in energy that the two isomers can co-exist. This is in contrast to the water adduct of UO_2^+, for which the physisorbed hydrate is distinctly more stable. The present computational results are in complete accord with these experimental observations: the physisorbed water adduct is 12 kcal/mol higher in energy for UO_2^+ whereas the physisorbed and chemisorbed water adducts are energetically degenerate for PaO_2^+, to within <1 kcal/mol. Furthermore, the observed faster oxo-exchange rate with water observed for PaO_2^+ versus UO_2^+ is predicted by the computed energetics in Figure 1. Specifically, the transition states for oxo-exchange are lower in energy than the reactant asymptotes by 1 kcal/mol and 7 kcal/mol for UO_2^+ and PaO_2^+, respectively, which results in much faster exchange for the latter.

Because of the necessity for a charge to study gas-phase species by mass spectrometry, water addition and oxo-exchange of neutral ThO_2 have not been experimentally examined. An interesting prediction of the computed energetics for water addition to ThO_2 is that oxo-exchange should be even more facile for ThO_2 than for PaO_2^+. This prediction is based on the energy of the transition state for ThO_2, which is 19 kcal/mol below the reactant asymptote. The

observation of water adducts for UO_2^+ and PaO_2^+ is a result of collisional and/or radiative cooling of the high-energy physisorption or chemisorption products; exchange occurs when cooling is insufficiently efficient to stabilize a high-energy adduct intermediate prior to dissociation. Under fully bi-molecular conditions, and absent radiative cooling on the reaction time scale, adduct formation would not be observed. Under low-pressure conditions, ThO_2 should very efficiently exhibit oxo-exchange with water, a prediction that is challenging to experimentally evaluate. Under high-pressure conditions that stabilize the lowest-energy products on the reaction pathway, the energies in Figure 1 predict that ThO_2 should readily hydrolyze to produce the chemisorption product, $ThO(OH)_2$. This predicted propensity of Th(IV) to readily hydrolyze is in accord with known solution and gas-phase chemistry of thorium.[65]

The computed reaction energies confirm that Pa(V) is at a turning point in the actinide series as regards the stabilities of the chemisorbed and physisorbed water-addition products in the gas phase. For Th(IV), chemisorption to produce hydroxyls is clearly favorable; for U(V), physisorption to produce hydrates is clearly favorable. For Pa(V) the two processes are essentially degenerate in energy. The intrinsic propensity of an actinide towards hydrolysis, equivalent in the present context to chemisorption, is key to its aqueous solution and sorption behavior. Computed gas-phase hydrolysis energetics can reveal parallels to known condensed phase chemistry,[16] suggesting that key factors which influence the propensity towards hydrolysis are apparent even in elementary monohydrates. The general parallel with solution hydrolysis of Th(IV) was noted above. However, a significant disparity between gas and solution chemistry is often introduced when directly comparing species with different charge states. In solution, hydrolysis strength exhibits a correlation with the charge density at the metal center, with the

result that UO_2^{2+} hydrolyzes more readily that UO_2^+,[65] the opposite of the predicted energetics for chemisorption vs. physisorption of a single water molecule (Figure 1). In the present study a particularly significant result is the comparative hydration/hydrolysis properties of PaO_2^+ and UO_2^+; because the charge states of these two species are the same, it is expected that bimolecular water addition should provide insights into differences between their aqueous solution properties. Guillaumont et al.[66] reported on the rapid solution hydrolysis of PaO_2^+ and postulated the hydrolytic species $PaO(OH)_2^+$, which is in contrast to later actinide dioxide cations, including UO_2^+, which are relatively stable towards hydrolysis. The present gas-phase computational and experimental[17] results reveal a direct parallel with this distinctive solution nature of PaO_2^+. Whereas $UO_2(H_2O)^+$ is 12 kcal/mol more stable than $UO_2(OH)_2^+$, $PaO_2(H_2O)^+$ and $PaO(OH)_2^+$ are essentially isoenergetic. The present results are thus in accord with the greater propensity for PaO_2^+ to hydrolyze, and provide a clear example of elementary molecular-scale chemistry revealing the underlying basis for chemistry observed in complex condensed phases.

Natural Population Analysis (NPA) The Natural Population Analysis based on the Natural Bond Orbitals (NBOs)[67,68] using NBO6[69,70] (Table 7) with wavefunctions calculated at the PW91/aug-cc-pVDZ(O,H)/cc-pVDZ-PP(M) density functional theory level using Gaussian09 shows that there is substantial backbonding into the *5f* and *6d* orbitals in ThO_2, with significantly more population in the *6d* than in the *5f*. The positive NPA charge on Th increases by about 0.25 e from ThO_2 to $ThO(OH)_2$ with decreases in both the *6d* and *5f* populations. In PaO_2^+, there are about 2 electrons in the *5f* and one electron in the *6d*. There is substantially more *5f* population than for the Th case with somewhat less *6d* population. The excess population can be considered to be due to backbonding from the ligands to the metal to generate an ion that resembles a Pa^{2+} that has lost both *7s* electrons or it can be considered to be a Pa^{2+} since the two formal O^{2-} cannot

Table 7. Summary of the Actinide NPA Populations.

Molecule	An oxidation state	q(An)	*5f*(M)	*6d*(M)
ThO_2	+4	2.04	0.75	1.31
$(H_2O)ThO_2$	+4	2.04	0.69	1.32
$ThO(OH)_2$	+4	2.30	0.59	1.17
PaO_2^+	+5	2.16	1.85	0.92
$(H_2O)PaO_2^+$	+5	2.36	1.81	1.02
$PaO(OH)_2^+$	+5	2.48	1.36	1.26
UO_2^{2+}	+6	2.81	2.56	0.94
$(H_2O)UO_2^{2+}$	+6	2.59	2.57	1.10
$UO(OH)_2^{2+}$	+6	2.56	2.54	1.10
$^2UO_2^{+,b}$	+5	2.31	3.02	0.88
$(H_2O)^2UO_2^{+,c}$	+5	2.21	2.96	0.98
$^2UO(OH)_2^{+,d}$	+5	2.32	2.75	1.03

[a] Calculated at the PW91/aug-cc-pVDZ(O,H)/cc-pVDZ-PP(M) level using the CCSD(T)//awT/wT-PP optimized geometries except for $ThO_2(H_2O)$, $^2UO_2(H_2O)^+$, and $^2UO(OH)_2^+$ which were optimized at CCSD(T)//awD/wD-PP level. There is ≤ 0.06 *7s* and ≤ 0.03 *7p* population on all actinides.
[b] $^2UO_2^+$: 5fα/β = 2.04/0.98, 6dα/β = 0.45/0.43
[c] $^2UO_2(H_2O)^+$: 5fα/β = 2.00/0.96, 6dα/β = 0.50/0.48
[d] $^2UO(OH)_2^+$: 5fα/β = 1.91/0.84, 6dα/β = 0.54/0.50.

pull enough electron density from the Pa to generate the +5 formal oxidation state. The positive charge on the Pa increases as H_2O is added, with a small change in the amount of electrons in the *5f* and *6d*. Transfer of the proton to form the two OH bonds in $PaO(OH)_2^+$ leads to a further increase in the positive charge on the Pa and a significant transfer of electrons from the *5f* to the *6d* as well as loss of electrons from the *5f* as the Pa becomes more positive. The population on the U in UO_2^{2+} continues this trend with ~ 2.6 e in the *5f* and 1 e in the *6d*. Thus the U in UO_2^{2+} looks like it has lost the two *7s* electrons and about 0.5 of a *5f* electron. Formation of the adduct leads to loss of positive charge on the U with an increase on the *6d*. There is no significant change in the populations from the adduct to the structure generated by proton transfer,

$UO(OH)_2^{2+}$. For the U in $^2UO_2^+$, there are almost 3 e in the *5f* and 1 e in the *6d*. Thus it closely resembles a U^{+2} with loss of the two *7s* electrons. Addition of the H_2O to form the Lewis acid-base adduct does not change the population too much with some transfer from the 5f to the 6d. Proton transfer to generate $^2UO(OH)_2^+$ has additional electron transfer from the 5f to the 6d. Thus the trends for $^2UO_2^+$ must closely follow those of PaO_2^+.

What could be correlated with the population analysis for these systems? It was somewhat surprising that there are real effects for the change in the orbitals used for the CCSD(T) calculations for the closed shell molecules and that there is a second order closed shell spin orbit contribution. We note that the effects of changing the orbitals and including the spin orbit correction are smallest (minimal) for ThO_2 and larger for the other An compounds. The populations in ThO_2 show the largest population in the *6d* and the lowest *5f* population. As the *5f* population on the An increases, there is a larger effect on the energy differences due to the change in the orbitals input to CCSD(T) and the second order spin orbit correction. We suggest that these effects are correlated and it is the increase in the amount of population of the *5f* orbitals that is responsible. This could happen as correlating the *5f* orbitals is likely to be the most difficult part of the calculation due to the different ways of populating these seven orbitals.

Conclusions

The potential energy surfaces for the reactions of H_2O with ThO_2, PaO_2^+, UO_2^{2+}, and UO_2^+ have been calculated at the coupled cluster CCSD(T) level extrapolated to the complete basis set limit with additional corrections including scalar relativistic and spin orbit. The reactions proceed by the formation of an initial Lewis acid-base adduct $(H_2O)AnO_2^{0/+/2+}$ followed by a proton transfer to generate the dihydroxide $AnO(OH)_2^{0/+/2+}$. For An = Th(IV) and Pa(V), the dihydroxide is symmetric and O isotope exchange in these species can occur without a barrier.

For An = U(V) and U(VI), the two hydroxyl groups are not equivalent and O isotope exchange in the dihydroxides occur with low barriers. For An = Th(IV), the dihydroxide is much more stable than the Lewis acid-base adduct with a low barrier to transfer the proton, consistent with predictions for the same processes in the Group 4 transition metals. For An = Pa(V), the Lewis acid-base adduct and the dihydroxide are isoenergetic within less than 1 kcal/mol, in excellent agreement with mass spectrometry experiments. The barrier to proton transfer is significantly higher than for rearrangement of the hydroxyl groups. For U(V), the proton transfer barrier is ~ 5 kcal/mol higher than for Pa(V) and the dihydroxide is 12 kcal/mol less stable than the Lewis acid-base adduct. For O exchange to spontaneously occur, the energy of the first proton transfer barrier must be below the energy of the reactant asymptote. The proton transfer barrier for U(V) is just (-0.3 kcal/mol) below the asymptotic limit, in agreement with the experimental observation of inefficient exchange. The proton transfer barrier for Pa(V) is significantly (- 6 kcal/mol) below the asymptotic limit, in accord with much faster exchange. The well depths for the Lewis acid-base adducts for the mono-cations are deeper than for Th. Removal of another electron to generate U(VI) leads to an even larger initial well-depth for the Lewis acid-base adduct, a further destabilization of the dihydroxide relative to the adduct and an increased barrier to proton transfer. However, the energy of the proton transfer transition state relative to the reactant asymptote is -10 kcal/mol for UO_2^{2+}, such that faster exchange is predicted, as has been experimentally observed.[71]

A number of interesting computational details presented themselves. Different input orbitals for the CCSD(T) calculations were found to improve the values relative to the use of the Hartree-Fock orbitals. The use of PW91 orbitals improved the results as did the use of Brueckner orbitals. The differences are beyond the normal chemical accuracy of ± 1 kcal/mol so they are

needed for quantitative predictions. It is important to note that these are for energy differences relative to the initial reactant asymptote. Furthermore, second order spin orbit corrections for closed shell molecules relative to the reactant asymptote were also necessary and are larger than ± 1 kcal/mol. On the basis of the NPA atomic populations, an argument was made that the amount of *5f* orbital character on the central actinide for the closed shell molecules played a role in the size of these corrections with larger *5f* character leading to larger corrections. The NPA analysis suggested that the Pa(V), U(V), and U(VI) in the actinyl ions, have *5f* and *6d* populations that are not far different from the those in the An(II) with two *7s* electrons lost.

Acknowledgement D.A.D acknowledges the support of the U.S. Department of Energy, Office of Basic Energy Sciences, Heavy Element Chemistry Program through a subcontract from Argonne National Laboratory. D.A.D. thanks the Robert Ramsay Fund at the University of Alabama. K.A.P acknowledges the support of the U.S. Department of Energy, Office of Basic Energy Sciences, Heavy Element Chemistry Program through Grant No. DE- FG02-12ER16329. The work of J.K.G. was supported by the U.S. Department of Energy, Office of Basic Energy Sciences, Heavy Element Chemistry, at LBNL under Contract No. DE-AC02-05CH11231.

Supporting Information. Complete references for 34, 48, and 49. Imaginary frequencies for transition states. Pa basis sets. Optimized XYZ Coordinates in Å. This material is available free of charge via the internet at http://pubs.acs.org.

References

[1] Crandall, H. W. The Formula of Uranyl Ion. *J. Chem. Phys.* **1949**, *17*, 602−606.

[2] Gordon, G.; Taube, H. J. The Uranium(V)-Catalysed Exchange Reaction Between Uranyl Ion and Water in Perchloric Acid Solution. *Inorg. Nucl. Chem.* **1961**, *16*, 272−278.

[3] Clark, D. L.; Conradson, S. D.; Donohoe, R. J.; Keogh, D. W.; Morris, D. E.; Palmer, P. D.; Rogers, R. D.; Tait, C. D. Chemical Speciation of the Uranyl Ion under Highly Alkaline Conditions. Synthesis, Structures, and Oxo Ligand Exchange Dynamics. *Inorg. Chem.* **1999**, *38*, 1456−1466.

[4] Szabo, Z.; Grenthe, I. Reactivity of the "yl"-Bond in Uranyl(VI) Complexes. 1. Rates and Mechanisms for the Exchange between the *trans*-dioxo Oxygen Atoms in $(UO_2)_2(OH)_2^{2+}$ and Mononuclear $UO_2(OH)_n^{2-n}$ Complexes with Solvent Water. *Inorg. Chem.* **2007**, *46*, 9372−9378.

[5] Szabo, Z.; Grenthe, I. On the Mechanism of Oxygen Exchange Between Uranyl(VI) Oxygen and Water in Strongly Alkaline Solution as Studied by ^{17}O NMR Magnetization Transfer. *Inorg. Chem.* **2010**, *49*, 4928−4933.

[6] Fortier, S.; Hayton, T. W. Oxo Ligand Functionalization in the Uranyl Ion (UO_2^{2+}). *Coord. Chem. Rev.* **2010**, *254*, 197−214.

[7] Wahlin, P.; Danilo, C.; Vallet, V.; Réal, F.; Flament, J. P.; Wahlgren, U. An Investigation of the Accuracy of Different DFT Functionals on the Water Exchange Reaction in Hydrated Uranyl(VI) in the Ground State and the First Excited State. *J. Chem. Theory Comput.* **2008**, *4*, 569−577.

[8] Réal, F.; Vallet, V.; Wahlgren, U.; Grenthe, I. Ab Initio Study of the Mechanism for Photoinduced Yl-Oxygen Exchange in Uranyl(VI) in Acidic Aqueous Solution. *J. Am. Chem. Soc.* **2008**, *130*, 11742−11751.

[9] Shamov, G. A.; Schreckenbach, G. Theoretical Study of the Oxygen Exchange in Uranyl Hydroxide. An Old Riddle Solved? *J. Am. Chem. Soc.* **2008**, *130*, 13735−13744.

[10] Schreckenbach, G.; Shamov, G. A. Theoretical Actinide Molecular Science. *Acc. Chem. Res.* **2010**, *43*, 19−29.

[11] Bühl, M.; Schreckenbach, G. Oxygen Exchange in Uranyl Hydroxide via Two "Nonclassical" Ions. *Inorg. Chem*. **2010**, *49*, 3821−3827.

[12] Bühl, M.; Wipff, G. Insights into Uranyl Chemistry from Molecular Dynamics Simulations. *ChemPhysChem*, **2011**, *12*, 3095−3105.

[13] Tsushima, S. "yl"-Oxygen Exchange in Uranyl(VI) Ion: A Mechanism Involving $(UO_2)_2(\mu\text{-}OH)_2^{2+}$ via $U\text{–}O_{yl}\text{–}U$ Bridge Formation. *Inorg. Chem.* **2012**, *51*, 1434−1439.

[14] Rabideau, S. W.; Masters, B. J. Oxygen Exchange Reactions of Plutonium Ions in Solution. *J. Phys. Chem.* **1963**, *67*, 318−323.

[15] Rabideau, S. W. The Oxygen Exchange Reactions of NpO_2^{+2} and NpO_2^{+} with Water. *J. Phys. Chem.* **1963**, *67*, 2655−2659.

[16] Rios, D.; Michelini, M. d. C.; Lucena, A. F.,; Marçalo, J.; Gibson J. K. On the Origins of Faster Oxo Exchange for Uranyl(V) versus Plutonyl(V). *J. Am. Chem. Soc.* **2012**, *134*, 15488−15496.

[17] P. D. Dau, R. E. Wilson, and J. K. Gibson Elucidating Protactinium Hydrolysis: The Relative Stabilities of $PaO_2(H_2O)^{+}$ and $PaO(OH)_2^{+}$. *Inorg. Chem.*, **2015**, *54*, 7474–7480.

[18] Fang, Z.; Dixon D. A. Computational Study of H_2 and O_2 Production from Water Splitting by using Small MO_2 Nanoclusters (M = Ti, Zr, Hf)," *J. Phys. Chem. A,* **2013**, *117*, 3539−3555.

[19] Fang, Z.; Outlaw, M.; Smith, K.; Gist, N.; Li, S.; Dixon, D. A.; Gole J. L. Computational Study of the Hydrolysis Reactions of Small MO_2 (M= Zr and Hf) Nanoclusters with Water. *J. Phys. Chem. C*, **2012**, *116*, 8475-8492.

[20] Wang, T.-H.; Fang, Z.; Gist, N. W.; Li, S.; Dixon, D. A.; Gole J. L. Computational Study of the Hydrolysis Reactions of the Ground and First Excited Triplet States of Small TiO_2 Nanoclusters. *J. Phys. Chem. C*, **2011**, *115*, 9344-9360.

[21] Peterson, K. A. Correlation consistent basis sets for actinides. I. The Th and U atoms. *J. Chem. Phys.* **2015**, *142*, 074105(14 pages).

[22] Purvis, G. D., III; Bartlett, R. J. A Full Coupled-Cluster Singles and Doubles Model: The Inclusion of Disconnected Triples. *J. Chem. Phys.* **1982**, *76*, 1910-1918.

[23] Raghavachari, K.; Trucks, G. W.; Pople, J. A.; Head-Gordon, M. A Fifth-order Perturbation Comparison of Electron Correlation Theories. *Chem. Phys. Lett.* **1989**, *157*, 479-483.

[24] Watts, J. D.; Gauss, J.; Bartlett, R. J. Coupled-Cluster Methods with Non-iterative Triple Excitations for Restricted Open-Shell Hartree-Fock and Other General Single-Determinant Reference Functions. Energies and Analytical Gradients. *J. Chem. Phys.* **1993**, *98*, 8718-8733.

[25] Bartlett, R. J.; Musial, M. Coupled-Cluster Theory in Quantum Chemistry. *Rev. Mod. Phys.* **2007**, *79*, 291-352.

[26] Dunning, T.H., Jr. Gaussian basiss set for use in correlated molecular calculations. I. The atoms boron through neon and hydrogen. *J. Chem. Phys*., **1989**, *90*, 1007-1023.

[27] Kendall, R. A.; Dunning, T. H., Jr.; Harrison, R. J. Electron Affinities of the First-Row Atoms Revisited. Systematic Basis Sets and Wave Functions. *J. Chem. Phys*. **1992**, *96*, 6796-6806.

[28] Dolg, M; Cao, X. Accurate Relativistic Small-Core Pseudopotentials for Uranium and First Applications to Uranium Hydride. *J. Phys. Chem. A* **2009**, *113*, 12573-12581.

[29] Weigand, A.; Cao, X.; Hangele, T.; Dolg, M. Relativistic Small-Core Pseudopotentials for Actinium, Thorium, and Protactinium. *J. Phys. Chem. A.* **2014**, *118*, 2519-2530.

[30] The corresponding correlation consistent basis sets for Pa are given in the current Supporting Information.

[31] Peterson, K.A.; Dunning, T.H., Jr. Accurate correlation consistent basis sets for molecular core-valence correlation effects: The second row atoms Al-Ar, and the first row atoms B-Ne revisited. *J. Chem. Phys*. **2002**, *117*, 10548-10560.

[32] Møller, C.; Plesset, M. S. Note on an approximation treatment for many-electron systems. *Phys. Rev.* **1934**, *46*, 618-622.

[33] Pople, J. A.; Binkley, J. S.; Seeger, R. Theoretical models incorporating electron correlation. *Int. J. Quantum Chem. Symp.* **1976**, *10*, 1-19.

[34] Frisch, M. J.; Trucks, G. W.; Schlegel, H. B.; Scuseria, G. E.; Robb, M. A.; Cheeseman, J. R.; Scalmani, G.; Barone, V.; Mennucci, B.; Petersson, G. A.; et al. *Gaussian 09*, revision B.01; Gaussian, Inc.: Wallingford, CT, 2009.

[35] Deegan, M. J. O.; Knowles, P. J. Perturbative Corrections to Account for Triple Excitations in Closed and Open Shell Coupled Cluster Theories. *Chem. Phys. Lett.* **1994**, *227*, 321-326.

[36] Rittby, M.; Bartlett, R. J. An Open-Shell Spin-Restricted Coupled Cluster Method: Application to Ionization Potentials in N_2. *J. Phys. Chem*. **1988**, *92*, 3033-3036.

[37] Knowles, P. J.; Hampel, C.; Werner, H.-J. Coupled Cluster Theory for High Spin, Open Shell Reference Wave Functions *J. Chem. Phys.* **1993**, *99*, 5219-5228.

[38] Peterson, K. A.; Woon, D. E.; Dunning, T. H., Jr. Benchmark calculations with correlated molecular wave function. IV. The classical barrier height of the $H+H_2 \rightarrow H_2+H$ reaction. *J. Chem. Phys.* **1994**, *100*, 7410-7415.

[39] Douglas, M.; Kroll, N. M. Quantum Electrodynamical Corrections to the Fine Structure of Helium. *Ann. Phys.* **1974**, *82*, 89-155.

[40] Jansen, G.; Hess, B. A. Revision of the Douglas-Kroll Transformation. *Phys. Rev. A* **1989**, *39*, 6016.

[41] Wolf, A.; Reiher, M.; Hess, B. A. The Generalized Douglas-Kroll Transformation. *J. Chem. Phys.* **2002**, *117*, 9215-9226.

[42] de Jong, W. A.; Harrison, R. J.; Dixon, D. A. Parallel Douglas-Kroll Energy and Gradients in Nwchem: Estimating Scalar Relativistic Effects Using Douglas-Kroll Contracted Basis Sets. *J. Chem. Phys.* **2001**, *114*, 48-53.

[43] Iliaš, M.; Saue, T. An Infinite-Order Two-Component Relativistic Hamiltonian by a Simple One-Step Transformation. *J. Chem. Phys.* **2007**, *126*, 064102(9 pages).

[44] Saue, T. Relativistic Hamiltonians for Chemistry: A Primer. *ChemPhysChem* **2011**, *12*, 3077-3098.

[45] Visscher, L.; Lee, T. J.; Dyall, K. G. Formulation and Implementation of a Relativistic Unrestricted Coupled-Cluster Method Including Noniterative Connected Triples. *J. Chem. Phys.* **1996**, *105*, 8769-8776.

[46] Kaldor, U. The Fock Space Coupled Cluster Method: Theory and Application. *Theor. Chim. Acta* **1991**, *80*, 427-439.

[47] Visscher, L.; Eliav, E.; Kaldor, U. Formulation and Implementation of the Relativistic Fock-Space Coupled Cluster Method for Molecules. *J. Chem. Phys.* **2001**, *115*, 9720-9726.

[48] Visscher, L.; Jensen, H. J. Aa.; Bast, R.; Saue, T. Dirac, a Relativistic Ab Initio Electronic Structure Program, Release Dirac13 (2013), http://www.diracprogram.org

[49] Werner H.-J.; Knowles, P. J.; Knizia, G.; Manby, F. R.; Schütz, M.; Celani, P.; Korona, T.; Lindh, R.; Mitrushenkov, A.; Rauhut, G.; MOLPRO, version 2012.1, a package of *ab initio* programs, See http://www.molpro.net.

[50] Werner H.-J.; Knowles, P. J.; Knizia, G.; Manby, F. R.; Schütz, M. Molpro: A General-Purpose Quantum Chemistry Program Package. *WIREs Comput. Mol. Sci.* **2012**, *2*, 242-253

[51] Perdew, J. P.; Wang, Y. Accurate and simple analytic representation of the electron-gas correlation energy. *Phys. Rev. B*, **1992**, *45*, 13244-13249.

[52] Perdew, J. P.; Burke, K.; Wang, Y. Generalized gradient approximation for the exchange-correlation hole of a many-electron system. *Phys. Rev. B*, **1996**, *54*, 16533-16539.

[53] Burke, K.; Perdew, J. P.; Wang, Y. Derivation of a generalized gradient approximation: The PW91 density functional in *Electronic Density Functional Theory: Recent Progress and New Directions*, Eds. Dobson, J.F.; Vignale, G.; Das M.P. Plenum, New York, 1997, 81-122.

[54] Brueckner, K. A. Nuclear Saturation and Two-Body Forces. II. Tensor Forces. *Phys. Re*v. **1954**, *96*, 508–516.

[55] Nesbet, R. K. Brueckner's Theory and the Method of Superposition of Configurations. *Phys. Re*v. **1958**, *109*, 1632–1638

[56] Larsson, S.; Smith, V. Analysis of the ^{2}S Ground State of Lithium in Terms of Natural and Best Overlap (Brueckner) Spin Orbitals with Implications for the Fermi Contact Term*Phys. Re*v. **1969**, *178*, 137–152.

[57] Chiles, R. A.; Dykstra, C. E. An electron pair operator approach to coupled cluster wave functions. Application to He_2, Be_2, and Mg_2 and comparison with CEPA methods. *J. Chem. Phys.* **1981**, *74*, 4544–4556

[58] Dykstra, C. E. Examination of Brueckner condition for selection of molecular-orbitals in correlated wavefunctions. *Chem. Phys. Lett.*, **1977**, *45*, 466-69.

[59] Handy, N. C.; Pople, J. A.; Head-Gordon, M.; Raghavachari, K.; Trucks, G. W. Size-consistent Brueckner theory limited to double substitutions. *Chem. Phys. Lett.*, **1989**, *164*, 185-92.

[60] Alexandrov, V.; Shvareva, T. Y.; Hayun, S.; Asta, M.; Navrotsky, A. Actinide Dioxides in Water: Interactions at the Interface. *J. Phys. Chem. Lett.* **2011**, *2*, 3130−3134

[61] Thanthiriwatte, K. S.; Vasiliu, M.; Battey, S. R.; Lu, Q.; Peterson, K. A.; Andrews, L.; Dixon, D. A. Gas Phase Properties of MX_2 and MX_4 (X=F, Cl) for M = Group 4, Group 14, Ce, and Th. *J. Phys. Chem. A*, **2015**, 119, 5790-5803

[62] Marçalo, J.; Gibson, J. K. Gas-phase thermodynamics of actinide oxides — an assessment of neutral and cationic monoxides and dioxides from thorium to curium. *J. Phys. Chem. A,* **2009**, *113*, 12599-12606

[63] Li, S.; Hennigan, J. M.; Dixon, D. A.; Peterson, K. A. Accurate Thermochemistry for Transition Metal Oxide Clusters. *J. Phys. Chem. A*, **2009**, *113*, 7861-7877

[64] Luo, Y.-R. *Comprehensive Handbook of Chemical Bond Energies*, CRC Press, Taylor and Francis Group, 2007.

[65] Choppin, G. R.; Jensen M. P. Actinides in Solution: Complexation and Kinetics, in *The Chemistry of the Actinide and Transactinide Elements, 3rd Ed.*, Morss, L. R.; Edelstein, N. M.; Fuger, J.; Eds., Vol. 4., Springer: Dordrecht, 2006, pp. 2524-2621.

[66] Guillaumont, R.; Bouissières, G.; Muxart, R. Chimie du Protactinium. I. Solutions Aqueuses de Protactinium Penta et Tetravalent. *Actinides Rev.* **1968**, *1*, 135-163

[67] Reed, A. E.; Curtiss, L. A.; Weinhold, F. Intermolecular Interactions from a Natural Bond Orbital, Donor-Acceptor Viewpoint. *Chem. Rev.* **1988**, *88*, 899-926.

[68] Weinhold, F.; Landis, C. R. *Valency and Bonding: A Natural Bond Orbital Donor-Acceptor Perspective*, University Press: Cambridge, U.K., 2005

[69] Glendening, E. D. ; Badenhoop, J. K.; Reed, A. E.; Carpenter, J. E.; . Bohmann, J. A; Morales, C. M.; Landis, C. R.; Weinhold, F. Natural Bond Order 6.0, Theoretical Chemistry Institute, University of Wisconsin, Madison, WI, 2013. http://nbo6.chem.wisc.edu/.

[70] Glendening, E. D.; Landis, C. R.; Weinhold, F. NBO 6.0: Natural Bond Orbital Analysis Program. *J. Comp. Chem.* **2013**, *34*, 1429-1437.

[71] Lucena, A. F.; Odoh, S. O.; Zhao, J.; Marçalo, J.; Schreckenbach, G.; Gibson J. K. Oxo-Exchange of Gas-Phase Uranyl, Neptunyl, and Plutonyl with Water and Methanol. *Inorg. Chem.*, **2014**, *53*, 2163–2170

TOC

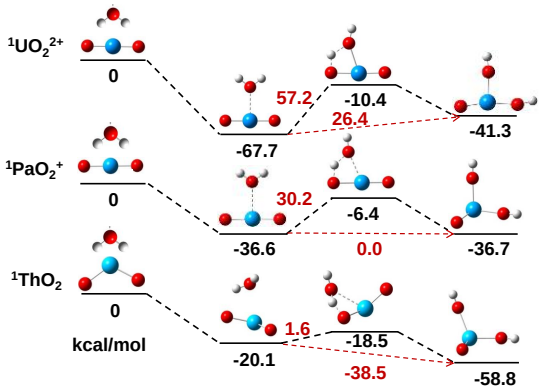
$^1UO_2^{2+}$
0
-67.7
57.2
-10.4
26.4
-41.3
$^1PaO_2^+$
0
-36.6
30.2
-6.4
0.0
-36.7
$^1ThO_2$
0
kcal/mol
-20.1
1.6
-18.5
-38.5
-58.8